Grain-boundary segregation of boron in high-strength steel studied by nano-SIMS and atom probe tomography

G. da Rosa, P. Maugis, A. Portavoce, J. Drillet, N. Valle, E. Lentzen, K. Hoummada

Full length article

Grain-boundary segregation of boron in high-strength steel studied by nano-SIMS and atom probe tomography

G. Da Rosa[a,b], P. Maugis[a,*], A. Portavoce[a], J. Drillet[b], N. Valle[c], E. Lentzen[c], K. Hoummada[a]

[a] Aix Marseille Univ, CNRS, IM2NP, Marseille, France
[b] ArcelorMittal Maizières Research SA, Voie Romaine, BP30320, 57283 Maizières les Metz, France
[c] Material Research and Technology Department, Luxembourg Institute of Science and Technology, 41 rue du Brill, 4422 Belvaux, Luxembourg

Keywords:
High-strength steel
Boron
Segregation
nano-SIMS
Atom probe tomography

High resolution imaging by secondary ion mass spectrometry and atom probe tomography have been employed to investigate boron segregation at austenite grain boundaries (γGBs) after soaking in a high-strength low-carbon steel. The combined use of these two analytical techniques is shown to be powerful for quantifying solute and segregated boron levels. Quenching was performed after soaking aiming to clarify the temperature effect on boron distribution under thermal equilibrium. Boron depletion in the γGBs vicinity was observed in the as-quenched states from high temperatures, suggesting that the cooling rate was not fast enough to limit boron diffusion during cooling. We found that boron segregation at γGBs increases with temperature. This is due to the increase of solute boron concentration in the grains, resulting from boride precipitate dissolution. It appears that the segregation magnitude still follows the equilibrium laws as a function of temperature. From our investigations, it was possible to determine the boron equilibrium segregation enthalpy. These results have important practical consequences for controlling the levels of segregated boron in steels.

1. Introduction

The addition of small amounts of boron (few tens parts per million – wt.ppm) has a positive effect on the hardenability of low-carbon steels [1]. This is commonly explained by B segregation at prior austenite grain boundaries (γGBs) delaying the austenite to ferrite phase transformation during cooling [2–7]. A similar effect has been observed on isothermal bainitic transformation [8]. The reason for this phenomenon is frequently attributed to the reduction of grain boundary energy due to B segregation, decreasing the number of heterogeneous sites for ferrite nucleation [9,10]. Depending on thermal cycle (soaking temperature, cooling rate, and final cooling temperature), B segregation can be controlled either by equilibrium (Equilibrium Segregation - ES) or non-equilibrium mechanisms (Non Equilibrium Segregation - NES) [11,12]. On the one hand, the driving force for ES is the decrease of the system total energy caused by solute atom migration from the matrix to the structural defects [13]. For the same solute concentration in a given solid solution, the ES magnitude decreases with increasing temperature, as will be discussed later. On the other hand, NES results from the formation of solute-vacancy complexes within the matrix [11,14–16]. When an alloy is first maintained at a soaking temperature and then cooled down to a lower temperature, vacancy (Va) concentration gradients appear in the vicinity of vacancy sinks. Oversaturated vacancies diffusing down this gradient drag the solute atoms toward the vacancy sinks via the solute-vacancy complexes. Since the equilibrium vacancy concentration increases with temperature, the number of vacancies liable to drag solute atoms is larger at higher soaking temperatures. In addition, boron-vacancy complexes (BVa) are generally considered to diffuse without limitation in the high temperature range [17]. Thus, contrasting with ES, NES magnitude increases with increasing soaking temperature [18,19]. Moreover, as NES depends on solute-vacancy complex diffusion to extended defects, the cooling rate is expected to play an important role on NES kinetics [15,26]. Most of the works on this topic indicate that NES becomes the dominant mechanism when increasing soaking temperatures (above 950 °C). As result of NES, the B segregation amount increases [16,18–21].

The study of B atomic distribution in steels is challenging. Indeed, the low B amount and its heterogeneous distribution require characterization techniques combining high sensitivity and high spatial-resolution. B segregation mechanisms have been studied in the past using particle tracking autoradiography (PTA) and conventional secondary ion mass spectrometry (SIMS) [2–4,8,18]. These techniques provide an overview of solute distribution at the micron scale. However, the lateral resolution of these tech-

* Corresponding author.
E-mail addresses: philippe.maugis@im2np.fr, philippe.maugis@univ-amu.fr

niques is insufficient to distinguish B segregation from small B-containing precipitates (below 50 nm). Furthermore, they are not the most appropriate techniques for quantitative analyses. Recent investigations of B distribution in steels have been carried out by high-resolution SIMS imaging (nano-SIMS) and/or atom probe tomography (APT) [6,7,22–24]. On the one hand, high-resolution SIMS has an excellent detection limit (a few ppm) and provides an overview of B distribution with a better lateral resolution (down to 50 nm) than conventional SIMS and PTA. On the other hand, APT provides precise information on solute distribution and concentration at grain boundaries. For example, Drillet et al. [23] investigated the effect of austenite recrystallization on B precipitation at γGBs by SIMS nano-analyses. With the same technique, Christien et al. [25] have successfully studied sulfur equilibrium segregation at γGBs. Other works allowed the B concentration at γGBs to be quantified at 930 °C using APT [6,7]. Recently, Takahashi et al. [26] investigated the Mo and cooling rate effects on the amount of B segregation at γGB by APT. So far, however, B segregation phenomena have been explained using qualitative data or using only the B amount measured at grain boundaries. Furthermore, the influence of both ES and NES mechanisms being directly related to B mobility, accurate values of diffusion coefficients are needed to discuss the mechanisms quantitatively.

The proper study of B segregation requires quantifying both concentrations of B atoms in solid solution in the grains and at the γGBs. APT is usually considered as the most suitable technique for investigating solute segregation in grain boundary vicinity. However, APT detection limit (about 40 at.ppm) may prevent B concentration measurements in grains. In contrast, although being generally only qualitative, nano-SIMS gives access to trace element concentrations as low as those expected in grains. Consequently, the combined use of these two analytical techniques appears to be the best way to investigate B segregation in steels.

In the present work, nano-SIMS and APT techniques were used to investigate boron grain boundary segregation as a function of temperature in a high-strength low-carbon steel. The nano-SIMS signals from the solid solution were calibrated by the APT measurements, allowing the quantification of very low concentrations of B. APT allowed the quantification of the segregated amount of B at grain boundaries by the interfacial excess measured via the integral profile. Using this experimental approach, both B amounts in γGBs and in solid solution in grains were quantified after different soaking temperatures. The equilibrium segregation mechanism is shown to be compatible with our experimental data. The B diffusion coefficient in austenite as well as the B equilibrium segregation enthalpy at austenite grain boundaries were deduced from these data.

2. Experimental

The material under investigation is a model alloy of advanced high-strength steel of composition Fe-0.075C-2.5Mn-0.0020B-0.02Ti in wt.% (or Fe-0.34C-2.45Mn-0.0100B-0.03Ti in at.%). The chemical composition results from boron addition to a low-carbon steel, with high manganese content aiming to decrease austenite formation temperature and to enhance hardenability. The presence of Ti is required to prevent B from precipitating with N [27–29]. Since micro-alloying elements were claimed to have a significant impact on B segregation, the addition of common micro-alloying elements (i.e. Mo and Nb) was intentionally avoided [3,4,8,18,30].

Cast ingots were initially hot-rolled, continuously cooled at −30 °C/h after 560 °C to simulate coiling, and then cold-rolled in the form of 1.3 mm thick sheets. At this stage, the microstructure consisted of ferrite and martensite. After cold-rolling, the samples were grounded in order to reduce their thickness to improve the quenching cooling rate after soaking. Subsequently, heat treatments were carried out on a Bähr DIL805 dilatometer to study B segregation under thermal equilibrium conditions. This apparatus provides accurate measurements over a wide range of heating and quenching rates. A type S thermocouple was welded on the sample surface allowing the temperature to be registered every 1 ms. The specimens were soaked at different temperatures (780 to 1100 °C) and then cooled down to room temperature. The soaking time was 600 s for the soakings ranging from 780 °C to 1000 °C and 120 s for the soaking at 1100 °C. The cooling rate after soaking was the maximum possible (approximately 500 °C s^{-1} within the first second of quenching) aiming at freezing the B equilibrium distribution existing at soaking temperature. After quenching, the samples were prepared for focused ion beam scanning electron microscopy (FIB - SEM). Since the cooling rate was very fast and, consequently, the temperature was not homogeneous in the entire sample, the APT and nano-SIMS analyses were performed in a region close to the thermocouple (~300 µm) and at ¼ of thickness of the cold rolled sheet.

SIMS analyses were carried out with a CAMECA NanoSIMS 50. This is an ion microprobe optimizing secondary ion analysis at high lateral resolution. The instrument was operated with a Cs^+ primary ion beam in order to analyze B and C as negative ions: $^{11}B^{16}O^-$ and $^{12}C^-$ respectively. Pre-sputtering of the surface was performed before each measurement in order to minimize C and O surface contamination. The different images, one for each ion, with a field of view of $20 \times 20\,\mu m^2$ were acquired simultaneously. The acquisition time was about 10 min. In order to compare quantitatively the different samples, all the analyses were done during the same analysis campaign to ensure similar analytical conditions. APT specimens were prepared using a dual-beam FIB-SEM. The APT analyses were carried out in a LEAP 3000X-HR instrument with electrical pulsing mode (100 kHz). The detection rate was kept to 0.002 event/pulse by increasing progressively the applied voltage. The specimen temperature and the fraction of pulsing were set to 70 K and 20% of applied voltage, respectively. Boron-containing ions were detected at mass over charge ratio $M/n = 5$ and 5.5 Da (B^{2+}), and at $M/n = 10$ and 11 Da (B^+). Regarding the volume reconstruction, we assumed that the grain boundaries are flat surfaces. In this way, we adjusted the compression factor ξ and the field factor k_F to obtain flat interfaces.

3. Results and discussion

3.1. Comparison between APT and nano-SIMS analyses

Fig. 1 shows an example of nano-SIMS and APT analyses of a sample after complete austenitization at 1100 °C for 120 s followed by quenching to room temperature. On the one hand (Fig. 1a), BO^- ion mapping obtained by nano-SIMS reveals the spatial distribution of boron in the microstructure, which consists of martensite. Although the martensite contains various boundaries, such as the γGBs, the newly formed packet, block, and laths, B segregation is only observed at the γGBs. The B-containing precipitates are also observable as bright spots (red and orange arrows), and the B atoms dissolved in the matrix are indicated by the light signal in the background (blue circles). On the other hand (Fig. 1b and e), APT confirms B segregation in a γGB and also reveals C segregation at the same grain boundary. Carbon segregation can also be observed at a second interface in the same volume (black arrow in Fig. 1b). This interface is probably a newly formed interface during martensitic transformation since it is free of boron. As already observed by nano-SIMS, 5 APT volumes, obtained from the grain interior, show that boron is homogeneously distributed. This result, already noticed by Li et al. [6,7], was reproduced in all APT analyses of this work. Boron is absent from the boundaries newly formed during martensitic transformation because its segregation

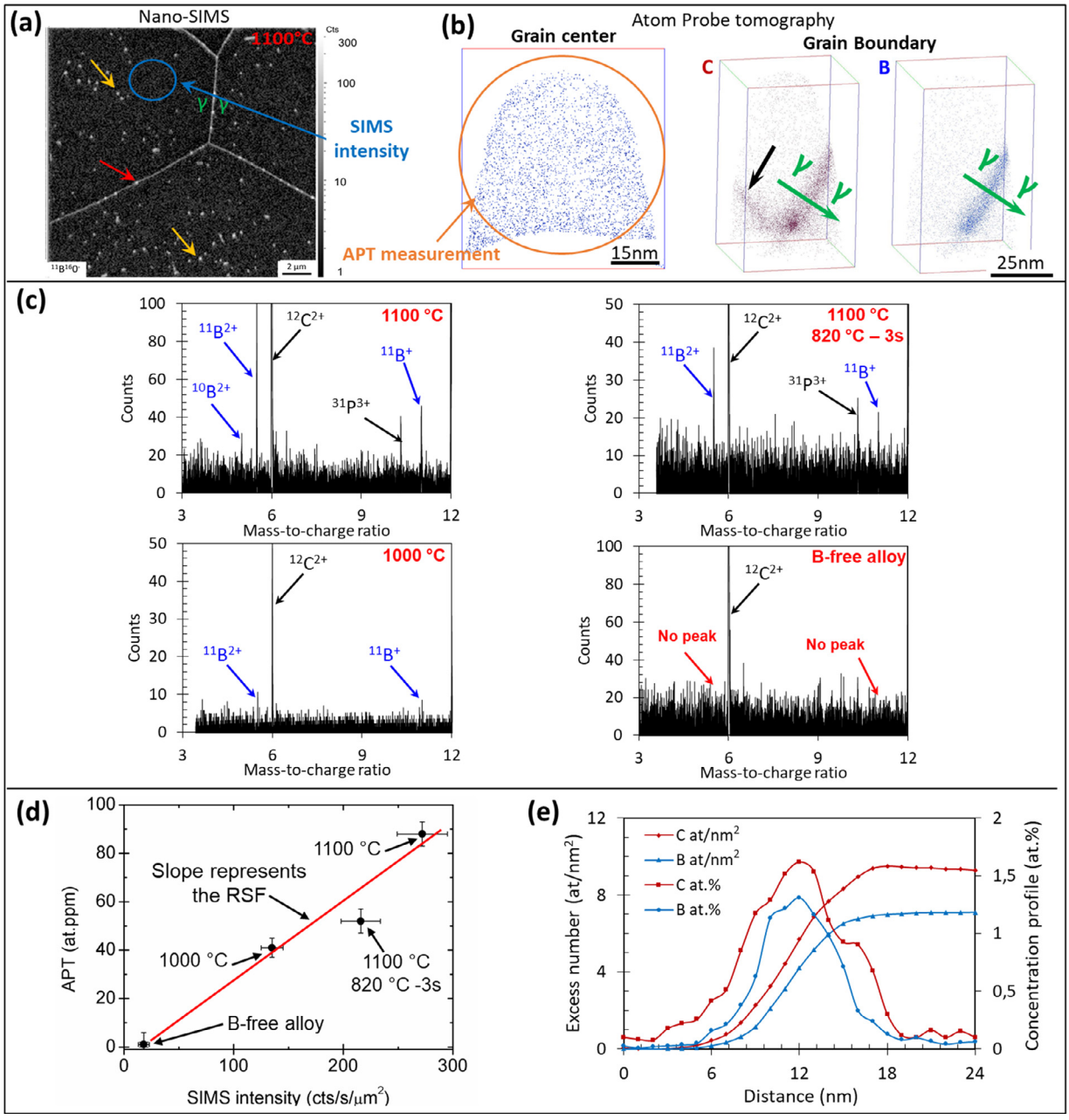

Fig. 1. Methodology of B quantification by APT and SIMS nano-analysis in grains and at grain boundaries (a) BO^- nano-SIMS map showing an overview of the B distribution. (b) APT volumes showing the local distribution of B in grains and B and C in the vicinity of an austenite grain boundary. (c) Part of APT mass spectra of the four samples used in the calibration curve showing P, B and C peaks (d) Calibration curve: B concentration in austenite grains measured by APT as a function of the BO^- ion intensity in grains obtained by SIMS nano-analysis. (e) Composition profiles and integral profiles across the γGB from the APT volume in figure (b) showing B and C excess numbers. Sample quenched after soaking at 1100 °C for 120 s.

is kinetically limited at low temperatures, below the martensitic transformation starting temperature ($T < 400$ °C).

It is possible to compare the B molar fraction X in different samples using the SIMS intensity. The relation between solute fraction and SIMS intensity is considered to be linear for solute fractions lower than 1 at% [31]. The proportionality factor RSF (Relative Sensitivity Factor) can be determined from the SIMS analysis of a standard sample containing a known concentration of the element of interest (Eq. (1)) [32]:

$$X = I \times RSF \quad (1)$$

This type of approach is routinely employed for in-depth conventional dynamic SIMS analysis, using a standard reference sample for concentration normalization. In our case, instead of using a reference sample, APT concentration measurements, performed each time on the same sample of interest as SIMS analyses, were used to calibrate the SIMS intensity. To validate our quantitative approach, the SIMS average intensity in the grains far from precipitates (Fig. 1a, blue circle) was compared with the concentration measured by APT (Fig. 1b, orange circle). To do so, three samples of the same steel but with different B concentrations in solution in austenite grains were analyzed by nano-SIMS and APT. It is worth mentioning that in order to detect B atoms in grains by APT, the samples needed to be heated at high temperatures to increase the solubility limit of B in the austenite. Two samples were soaked at 1000 °C and 1100 °C, respectively, followed by quenching to room temperature. The third sample was soaked at 1100 °C, then cooled down to 820 °C and held at this temperature

for 3 s before quenching to room temperature. A fourth sample with similar composition than the material under investigation, but without boron ($X < 15$ at.ppm, measured by optical emission spectroscopy), was also analyzed. The APT mass spectrum of these four samples can be seen in Fig. 1c: the peaks corresponding to boron are visualized in the three samples containing B. In contrast, in the B-free alloy we do not see the B peaks, as expected. The SIMS average intensity was computed from the average of different grains, the standard deviation of SIMS intensity being around 10%. This small variation indicates that the impact of grain orientation on SIMS intensity is small and, therefore, can be neglected in this work. The total surface analyzed for each sample was about 80 μm^2. Boron was found homogenously distributed in all the grains analyzed by APT, and the standard variation of B concentration between different volumes of a same sample was found to be about 5%. Fig. 1d shows that the SIMS intensity versus B concentration measured by APT can be fitted with a linear law. The RSF computed from this curve allows the concentration of B atoms in solid solution to be determined from nano-SIMS data, with a better detection limit than that of APT.

The calibration is more complex at grain boundaries. Indeed, the amount of segregation is usually quantified experimentally by the peak value of the concentration profile across the boundary. However, it was shown that the most adequate procedure to quantify solute segregation is via the interfacial excess of solute. It is calculated from the integral of a concentration profile measured across the boundary when the boundary is in local equilibrium with the bulk [33–36] . However, B concentration at γGBs usually exceeds 1 at.% making SIMS quantification more difficult due to the matrix effect on B ionization. Thus, the RSF for B could have different values in the grain boundaries than in the grains. Therefore, despite what has been done in the literature [25], we should not retrieve the interfacial excess of solute from a SIMS intensity profile across the boundary (see Eq. (1) in [34]). Instead, we measured the interfacial excess quantities from APT concentration profiles. The integral profiles (Fig. 1e) clearly exhibit C and B segregation in the sample annealed at 1100 °C: the interfacial excess numbers for C and B atoms were found to be 9.2 at.nm^{-2} and 7.1 at.nm^{-2}, respectively.

In order to follow B segregation at different soaking temperatures T_{soak}, other samples (soaked at 780, 790, 820, 860, and 1000 °C for 600 s) were analyzed by nano-SIMS and APT. The microstructure consisted of 80% of austenite and 20% of ferrite at 780 °C and 90% of austenite and 10% of ferrite at 790 °C, while the microstructure was fully austenitic at 820 °C and higher temperatures. The austenite grain size varies from 6 µm to 55 µm for the temperature range of 780 °C to 1100 °C. B maps obtained by nano-SIMS of the samples soaked at 790, 820, 860, and 1000 °C are shown in Fig. 2. After soaking at 790 °C, B has clearly segregated at γGBs. It is also present in precipitates (white dots indicated by purple arrows). B is known to co-precipitate with C resulting in the formation of B-containing cementite during annealing [37–39]. One can note that when the soaking temperature increases, the density of the B-containing precipitates (white dots), decreases up to 860 °C. However, after soaking at 1000 °C, the density of intragranular precipitates increases, but these white dots are smaller and of lower SIMS intensity, suggesting that these precipitates are smaller (yellow arrow). The presence of Fe_2B and $M_{23}(B,C)_6$ particles in low-carbon steels in the austenitic domain has been reported by several authors [28,29,37,40]. Furthermore, B-containing precipitates (red arrow) at γGBs, commonly identified as $M_{23}(B,C)_6$ [4,18,23], start to appear at this temperature. These precipitates were probably formed during quenching after soaking due to high B diffusivity at high temperatures. At the same time, the SIMS intensity in the grain (blue circle) increases with increasing temperature. After calibration by APT measurements, B in solid solution in grains was found to increase from 16 at.ppm to 90 at.ppm with increasing soaking temperature from 780 °C to 1100 °C (Fig. 3b). This result is explained by the total dissolution of the B-containing cementite and $M_{23}(B,C)_6$ particles and from the solubility of the remaining Fe_2B particles in austenite [37].

Six grain boundaries were analyzed by APT for the soaking performed at 820 °C: the excess numbers were found remarkably constant, lying in the range of 3.6 to 3.9 at.nm^{-2}. At 780 °C, 860 °C, and 1100 °C the interfacial excess are respectively 3.8 at.nm^{-2}, 5.9 at.nm^{-2}, and 7.1 at.nm^{-2}. Fig. 3a shows the corresponding integral profiles. Fig. 3b shows the evolution of B concentration in solid solution in grains (nano-SIMS measurements) and the excess numbers at γGBs (APT measurements) as a function of the soaking temperature. These results show that both B segregation level and solute B concentration increase with the soaking temperature.

The combined use of nano-SIMS and APT proved to be powerful to quantify B distribution in our steels. On the one hand, the APT technique yielded the B distribution at grain boundaries thanks to its unique capability to combine atomic-scale spatial resolution with chemical analysis; and on the other hand, nano-SIMS imaging gave access to the B trace concentration in the grains thanks to its excellent detection limit, using APT for concentration calibration. Nano-SIMS also provided a large-scale overview of B distribution in the microstructure, showing the presence of B precipitates, for example.

3.2. Modelling boron segregation kinetics

Boron equilibrium segregation is known to be reached in γGBs after a few minutes of high-temperature soaking (above 750 °C). Subsequent efficient quenching is thus expected to freeze an equilibrium flat concentration profile of boron up to the γGB location, where the boron enrichment makes a peak. In order to measure the equilibrium boron concentration in solid solution in the grain, concentration profiles were measured through γGBs after soaking and quenching. Fig. 4 shows such profiles measured by nano-SIMS after quenching from 820, 860, 1000, and 1100 °C. The profiles corresponding to the highest temperatures (1000 and 1100 °C) present significant depleted zones of several microns in the γGB vicinity. The existence of depleted zones suggests that boron atoms diffused towards the grain boundary during quenching. The driving force for such diffusion is the higher equilibrium segregation level at lower temperature, according to McLean's law. Depletion is not to be excluded at lower soaking temperatures but could not be observed by nano-SIMS analyses, the lateral resolution being of the order of 150 nm in our analytical conditions.

We built a numerical model to investigate the diffusion and segregation kinetics of boron during soaking and quenching. Fitting of the model against the measured concentration profiles and interface excess values allowed retrieving the segregation Gibbs energy as a function of temperature. The model is described below. Boron diffusivity along the grain boundaries is most probably a few orders of magnitude faster that in the bulk. Hence, during segregation, boron composition in the grain boundary remains uniform. This allows for the use of a one-dimensional model of segregation-diffusion toward the boundaries. At any point in the bulk, the diffusion flux of boron atoms was described by the Onsager law involving the atom mobility M and the chemical potential per atom μ:

$$J = -M\frac{\partial \mu}{\partial x}, \tag{2}$$

where x is the distance to the boundary. From the mass balance, the kinetic equation was written

$$\frac{\partial X}{\partial t} = -V_m\frac{\partial J}{\partial x}. \tag{3}$$

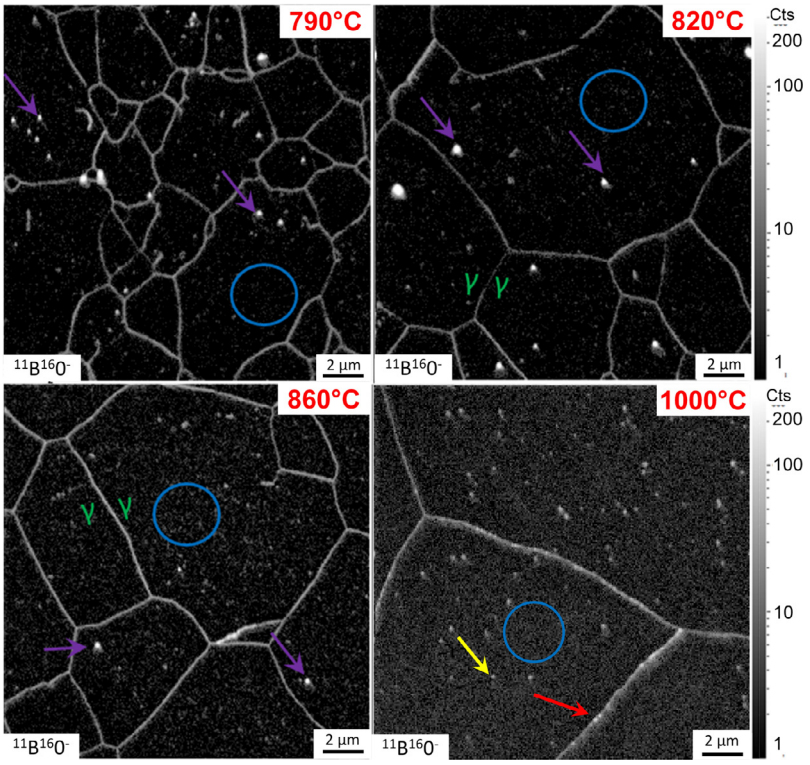

Fig. 2. BO^- nano-SIMS map showing B segregation at prior austenite grain boundaries, B in intragranular precipitates (purple and yellow arrows) and the presence of B at grain boundaries (red arrow). The specimens were quenched after 600 s of soaking at different temperatures indicated in each figure. (For interpretation of the references to colour in this figure legend, the reader is referred to the web version of this article.)

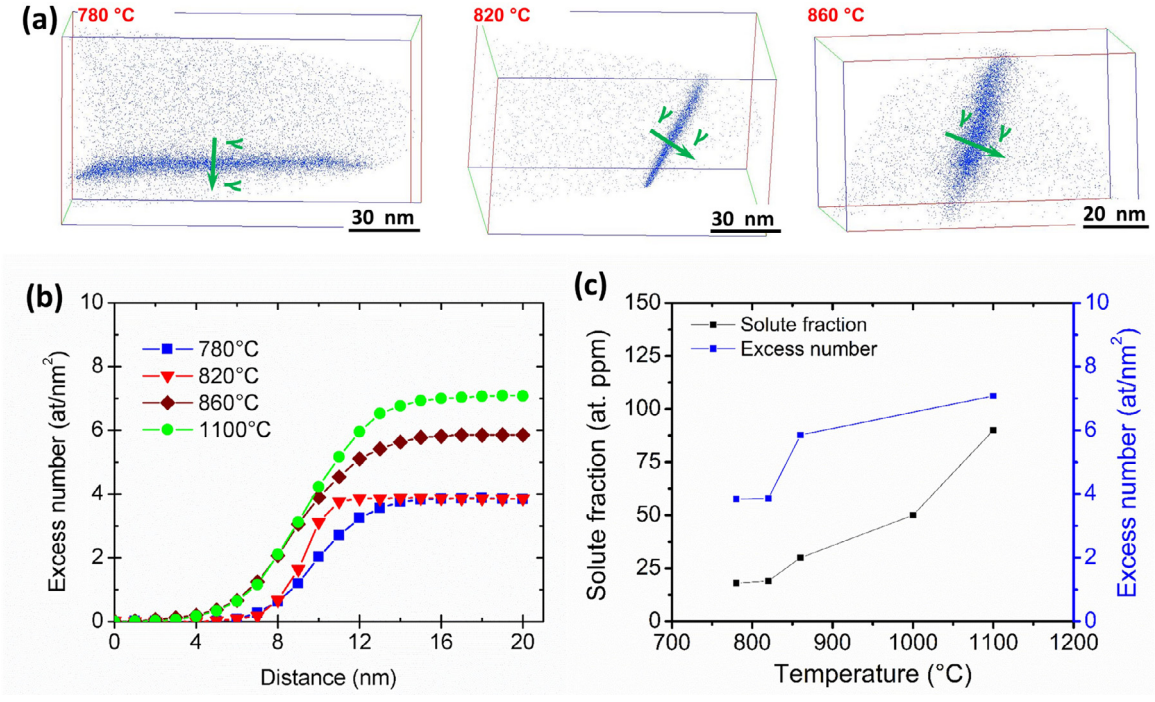

Fig. 3. (a) Reconstructed APT volumes after three soaking temperatures. (b) Boron integral profiles measured by APT giving the excess numbers in at.nm^{-2} at γGBs for four different soaking temperatures. (c) Boron concentrations in solid solution measured in the grain center by nano-SIMS (black squares, left axis); and excess numbers at γGB measured by APT (blue squares, right axis), as a function of soaking temperature. (For interpretation of the references to colour in this figure legend, the reader is referred to the web version of this article.)

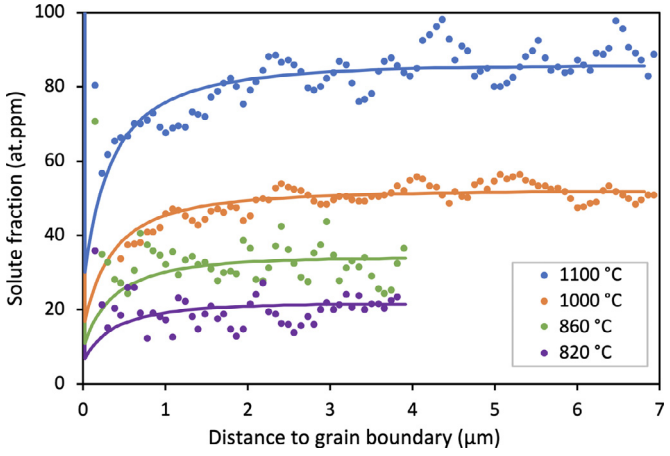

Fig. 4. Concentration profiles of boron measured by SIMS (points) from the center of austenite grain to the boundary, after soaking at different temperatures and quenching. The solid lines correspond to the kinetic model.

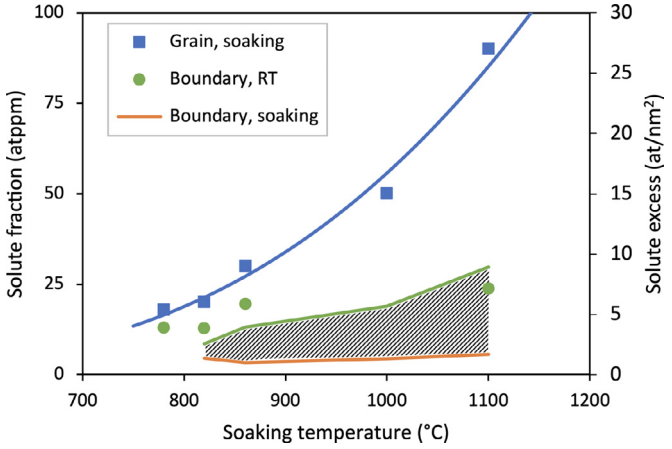

Fig. 5. Distribution of boron at the end of soaking and after quench. Solute fraction in the grains (blue, left axis) and excess numbers at grain boundaries (green and orange, right axis). The orange line is the computed excess at the end of the soaking stage. The green points and line refer to resp. the measured and computed excess after quench. The hatched region highlights the quantity of boron segregated during the quench. (For interpretation of the references to colour in this figure legend, the reader is referred to the web version of this article.)

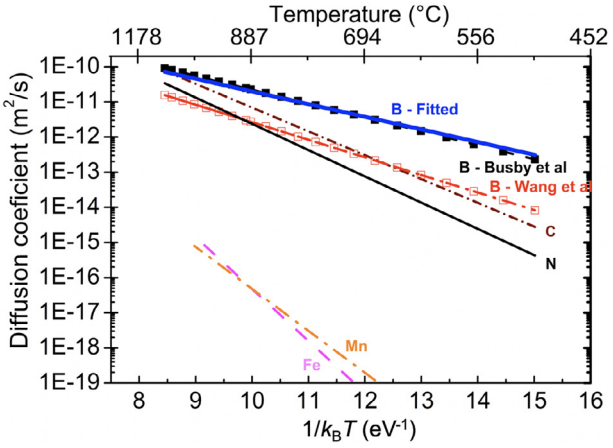

Fig. 6. Diffusion coefficients of B, C, Mn and Fe in austenite [41,44–47].

where V_m is the molar volume of the alloy. To compute the mass balance at the grain boundary, a boundary thickness equal to one lattice parameter (0.35 nm) was assumed. As far as the interaction of boron atoms with substitutional elements is negligible, the alloy thermodynamics of interstitial boron can be approximated to an ideal solution on the sublattice of the octahedral sites of the fcc host lattice. Then the chemical potential of boron was written under the classical form

$$\mu = k_B T \ln \frac{X}{1-X}. \quad (4)$$

In this equation, X is strictly the number of boron atoms per substitutional atom. On account of the low boron content, X can be approximated to the atom fraction of boron.

At the grain boundary, the chemical potential is augmented by the Gibbs energy of segregation ΔG_{seg}:

$$\mu = k_B T \ln \frac{X}{1-X} + \Delta G_{seg} \quad (5)$$

Eq. (5) is McLean's equation, with $\Delta G_{seg} = \Delta H_{seg} - T\Delta S_{seg}$. The mobility M is classically related to the diffusivity D by the relation

$$M = \frac{D}{k_B T} \frac{X(1-X)}{V_m} \quad (6)$$

Diffusion is thermally activated according to

$$D = D_0 \exp \frac{-Q}{k_B T} \quad (7)$$

where D_0 is the pre-exponential term, Q the activation energy and k_B the Boltzmann constant.

A one-dimensional finite difference scheme was applied to solve the diffusion-segregation equations for boron atoms. A line crossing the boundary between two neighboring grains was discretized, and the zero-flux boundary condition was applied at the center of the grains. The initial condition is a uniform distribution of boron in solid solution. The diffusion profiles as a function of time were computed during soaking and quenching (−500 °C/s down to 350 °C, i.e. the temperature of 50% martensitic transformation). To compare with experiments, the solute fractions computed at the grain boundary were converted to solute excess according to the procedure detailed in Section 3.4 (Eq. (9)). Fitting the segregation entropy and enthalpy gave $\Delta S_{seg} = 0.27$ eV/K and $\Delta H_{seg} = -0.39$ eV.

All calculated diffusion profiles at the end of the thermal cycle exhibit solute depleted zones in the vicinity of the grain boundary (Fig. 4). Examination of the kinetics of segregation at the grain boundary shows that most part of the segregation occurs during the quench (Fig. 5, hatched region). In fact, at the temperatures of soaking the driving force for segregation is low and the resulting equilibrium excess is small. The driving force increases during the quench, and segregation is fed by the high diffusivity of boron, even at moderate temperatures.

3.3. Boron diffusion in austenite

Busby et al. [41], measured the diffusion coefficient of boron in austenite and found $D_0 = 2 \times 10^{-7}$ m^{2}s^{-1} and $Q = 0.91$ eV. Takahashi et al. [26] successfully modelled the segregation kinetics in various boron-containing steels using these data. Here, to provide the best fit of our diffusion profiles we adopted the slightly different values $D_0 = 8 \times 10^{-8}$ m^2.s^{-1} and $Q = 0.83$ eV. They however lead to a similar temperature dependence as Busby's data. Fig. 6 and Table 1 present the diffusion coefficients of B compared to the literature for C and N atoms (direct interstitial mechanism) and Fe and Mn atoms (vacancy mechanism). Boron diffusion is found to be much faster (at least five orders of magnitude) than Mn and Fe diffusion, suggesting that B diffusion is interstitial-mediated in austenite. It is also faster than C and N diffusion. Considering the larger atomic radius of B compared to C and N, one may anticipate that B would

Table 1
Diffusion activation energies of different elements measured in austenite (in eV).

Direct vacancy mechanism		Direct interstitial mechanism				
Fe [46]	Mn [46]	N [47]	C [45]	B [this work]	B [44]	B [41]
3.4	2.75	1.72	1.56	0.83	1.15	0.91

diffuse slower than C and N. However, the rule that larger atoms are slower is not always valid. For instance, the interstitial oxygen, although smaller than carbon, has a lower diffusivity in iron [42]. Also, Janotti et al. [43] showed by first-principle calculations that larger substitutional atoms can diffuse faster.

Notice that the B diffusion coefficient determined here was measured during quenching, which means that at each recorded temperature during cooling, the vacancy concentration may not be at thermodynamic equilibrium. Indeed, one can reasonably expect an oversaturation of vacancies during quenching. B diffusion using the direct interstitial mechanism in austenite, variations in vacancy concentration should not modify the diffusion coefficient of B. However, B is expected to use two different diffusion mechanisms: (i) the direct interstitial mechanism and (ii) a BVa pair mediated mechanism exhibiting a slower diffusion coefficient probably close to Fe self-diffusion, as for usual vacancy-mediated mechanisms [48]. Consequently, Va concentration variations could influence the effective B diffusion coefficient only through the variations of BVa pair concentration. Considering the BVa pair interaction energy $E_b = -0.5\,eV$ [49] and the vacancy formation energy $E_f = 1.4\,eV$ [49] in austenite, the equilibrium BVa pair fraction can be calculated as $X_{BVa} = 12\ X_B\ \exp[-(E_f + E_b)/k_B T]$ [16]. At $T = 1100\,°C$ the fraction of B atoms using the BVa mechanism is found to be $X_{BVa}\ /\ X_B = 0.006$, which is negligible compared to the rest of B atoms using the direct interstitial mechanism. In addition, the diffusion coefficient of BVa pairs is expected to be smaller than the B direct interstitial diffusion coefficient. In fact, knowing the Fe activation energy (Table 1) and the BVa pair binding energy, the BVa pair activation energy can be calculated, assuming that the rate-limiting step for the diffusion of BVa is the migration of the vacancy, unaffected by its binding with boron. In fact, the activation energy of the BVa pair E_a^{BVa} is the formation energy of a pair $(E_f + E_b)$ added to the activation energy for migration of the vacancy (E_m). Since the activation energy for vacancy diffusion is $E_a = E_f + E_m = 3.4eV$, we finally have $E_a^{BVa} = E_a + E_b = 2.9eV$ [50,51]. This value is twice the activation energy of the effective diffusion coefficient of boron. Consequently, despite the quenching effect on vacancy concentration, even if the BVa formation mechanism may have a significant impact on B segregation in γGB, its effect on B diffusivity in our experimental conditions is negligible, the main part of B atoms using the direct interstitial mechanism to diffuse in austenite bulk. The effective B diffusion coefficient determined in our experimental conditions should be relatively similar to the equilibrium B direct interstitial diffusion coefficient.

3.4. Segregation energy

McLean's equation describing the equilibrium segregation of a solute atom on a defect [13] can be used to describe the equilibrium segregation state in the vicinity of a grain boundary through the segregation ratio N/N_{max} and the Gibbs free energy of segregation ΔG_{seg}. N is defined as the number of segregated solute atoms, while N_{max} is the number of so-called "favorable sites" into which the solute atoms may segregate. A grain boundary is saturated in solute when N reaches the value N_{max}. N and N_{max} bear the unit of a number of atoms (resp. sites) per unit area of grain boundary. With these notations, McLean's segregation equation writes

$$\frac{N}{N_{max} - N} = \frac{X}{1 - X} \exp\left(-\frac{\Delta G_{seg}}{k_B T}\right) \tag{8}$$

where X is the fraction of solute in solid solution in the grain boundary vicinity. The quantity N is related to the excess of solute Γ via the equation [34]

$$\Gamma = N - N_{ss}, \tag{9}$$

where N_{ss} is the value of N if no segregation had occurred, i.e. when $\Gamma = 0$. In the dilute solid solution under study, N_{ss} is negligible compared to N, and hence Γ is identical to N. Then, having defined $\Gamma_{max} = N_{max}$, McLean's segregation equation (Eq. (8)) can be rewritten

$$\frac{\Gamma}{\Gamma_{max} - \Gamma} = \frac{X}{1 - X} \exp\left(-\frac{\Delta G_{seg}}{k_B T}\right). \tag{10}$$

If the favorable sites are far from being saturated, viz. $\Gamma << \Gamma_{max}$, and when the solid solution is dilute, viz. $X << 1$, Eq. (10) reduces to

$$\frac{\Gamma}{\Gamma_{max}} = X\ \exp\left(-\frac{\Delta G_{seg}}{k_B T}\right), \tag{11}$$

which is known as the Langmuir equation [52]. Γ was measured using APT, X was measured using nano-SIMS/APT, and the number of favorable sites Γ_{max} can be derived from a structural model of the interface. Considering the sites occupied by B atoms in the matrix, we assumed that the favorable sites for the segregation of B atoms are the octahedral interstitial sites [44] located in the range of two interplanar spacings around the grain boundary [53]. In the (100) direction, this corresponds to a distance equal to the lattice parameter a. Considering that each substitutional site of the fcc lattice is associated to one octahedral interstitial site, the total surface density of favorable sites is 4 sites per fcc unit cell, giving $\Gamma_{max} = 4/a^2 = 32.7\ at.nm^{-2}$ with $a = 0.35\,nm$.

The diffusion-limited equilibrium segregation model, proposed by Takahashi et al. [26], shows that the grain boundary concentration of B increases during continuous cooling, following McLean's equilibrium equation in the high temperature range above 850 °C. Below this temperature, the grain boundary concentration of B cannot anymore follow the equilibrium, but continues to significantly increase, even for cooling rate of 640 °C/s. Since the equilibrium could not be reached at lower temperatures, a depleted zone should appear in the grain boundary vicinity. Our experiments show a similar behavior. In addition, we conclude that most part of the segregated amount measured after quenching results from segregation occurring during the quench.

Carbon segregation is known to occur but is difficult to quantify due to carbon diffusion during quenching and storage at room temperature [54]. However, C segregation may influence B segregation by the co-segregation mechanism [55]. Therefore, the B segregation enthalpy determined here corresponds to B segregation in presence of C at austenite γGBs.

3.5. Temperature dependence of the boron distribution

Since small amounts of boron remarkably increase the hardenability of low-carbon steels, extensive studies have been devoted

Table 2
Boron segregation enthalpy and boron-containing precipitate dissolution enthalpy.

Enthalpies (eV)	ΔH_{seg}	ΔH_{diss}	$\Delta H_{seg} + \Delta H_{diss}$
Literature [56,57]	−0.59	+0.7	+0.11
This work	−0.39	+0.64	+ 0.25

to investigating the soaking temperature dependence on B distribution. The total amount of segregated B has been reported to increase with increasing soaking temperature. This increase is usually assumed to be due to non-equilibrium segregation, which is claimed to be more relevant at high soaking temperatures (> 950 °C).

We see from Fig. 5 that boron in solid solution increases with increasing temperature. The enthalpy of B precipitate dissolution was calculated from these data. We found $\Delta H_{diss} = +0.64$ eV. This value is in good agreement with the Fe_2B compound solubility in austenite, corresponding to $X = \exp(-67{,}375\,\mathrm{J.mol^{-1}}/RT\ -2.8763)$, i.e. $\Delta H_{diss} = +0.7$ eV [56]. Correlatively, the excess number also increases with increasing temperature (Fig. 5). The amount of segregated atoms following the equilibrium segregation mechanism is known to decrease with increasing temperature. In our case, due to B enrichment of the matrix resulting from precipitate dissolution, this amount may *increase* with temperature. In fact, the solubility limit can be written

$$X = X_0 \exp\left(-\frac{\Delta H_{diss}}{k_B T}\right) \tag{12}$$

where X_0 is a constant related to the entropy of dissolution: $X_0 = 0.0563$. Combining Eqs. (11) and (12) gives the temperature dependence of the interfacial excess:

$$\Gamma = \Gamma_0 \exp\left(-\frac{\Delta H_{seg} + \Delta H_{diss}}{k_B T}\right), \tag{13}$$

with the constant

$$\Gamma_0 = \Gamma_{max} X_0 \exp\left(\frac{\Delta S_{seg}}{k_B}\right), \tag{14}$$

$\Gamma_0 = 42.0$ at/nm^2, where ΔH_{seg} and ΔS_{seg} are respectively the enthalpy and entropy of segregation. The segregation magnitude depends on an apparent enthalpy equal to the sum of ΔH_{seg} (negative) and ΔH_{diss} (positive) from Eq. (13). As a consequence, if $|\Delta H_{seg}| < |\Delta H_{diss}|$, the sum is positive and the B concentration in γGBs increases with temperature. The segregation data from the present study are compared to the literature [56,57] in Table 2. In both cases, the precipitate dissolution enthalpy is larger than the segregation enthalpy. This way, B excess in austenite grain boundaries increases with temperature, still following the equilibrium segregation isotherm.

Since the amount of B in the alloy is very small and B strongly segregated at γGB, the variation of austenite grain size must also be discussed. It could have an impact on B segregation due to the consumption of B in solid solution when the grain is too small. The impact of austenite grain size on B content in solution, B segregated at γGB, and B as precipitates, can be described by $C_N = C_g + \frac{2}{d}\Gamma + C_P$ with $\Gamma = C_g K$, where C_N, C_g, and C_P are, respectively, the nominal solute content, the solute content in solution, and the solute content as precipitates, in at/nm^3. d is the austenite grain size, Γ is the excess number, and K is related to the segregation energy of boron. The ratio $2/d$ corresponds to the GB area/grain volume ratio, based on stereology. Using this formula, we confirm that the effect of austenite grain size can be neglected for austenite grain sizes greater than 1 µm, which is the case of our study.

It could be thought that NES mechanism also contributes to the increase of boron segregation with increasing soaking temperature. However, the increase was observed even in the low soaking temperature range, between 780 °C and 860 °C, where the vacancy concentration is very low (e.g. ~2 at.ppm at 860 °C) compared to B concentration. After soaking at 1100 °C, even though vacancy concentration becomes higher (~29 at.ppm), the fraction of BVa complexes is less than 1 at.ppm. In addition, one of the necessary conditions for NES to occur is that the complex diffusion be faster than B diffusion. For example, Williams et al. [49] and Faulkner [58] suggested a boron-vacancy complex diffusion coefficient 250 times faster than B interstitial diffusion. Otherwise, no accumulation of solute at γGBs should be expected. However, as mentioned in Section 3.2, it is unlikely that the diffusion coefficient of complexes, which uses the vacancy mechanism, be higher than the diffusion coefficient of B which uses the direct interstitial mechanism in austenite. For these reasons, the contribution of NES to boron segregation in these experiments can be neglected.

Recently, Myamoto et al. [59] using a similar approach as used in this work, also observed that B segregation at γGBs increases with increasing soaking temperature from 900 to 1050 °C and to 1200 °C. The authors suggest that NES occurs during cooling. Using conventional SIMS, they did not observe B precipitates at 1050 °C and at 1200 °C. However, due to the limited lateral resolution of conventional SIMS, it is not unlikely that small boride particles still exist in the high soaking temperature conditions: as can be seen in Fig. 2, even with high resolution SIMS, the signal of B precipitates is very low. This may explain the disagreement with our results.

4. Conclusions

The effect of temperature on boron atoms in solid solution in austenite and boron interfacial excess at austenite grain boundaries in a high-strength low-carbon steel were quantified using nano-SIMS and APT measurements. Our combined measurements, allowing high spatial resolution as well as high detection limit, were performed after quenching the samples from temperatures above 780 °C, at which the austenite phase is thermodynamically stable, down to room temperature. Quantitative data concerning grain boundary segregation in austenite could be obtained using a numerical model of coupled diffusion and segregation phenomena. In summary, the present study revealed that:

(1) APT and nano-SIMS techniques allow quantifying very small quantities of boron in solid solution, as well as precise amounts of boron segregated at grain boundaries. The combined use of these two analytical techniques is essential for a complete understanding of B segregation in low-carbon steels.
(2) Boron atoms are very mobile at high temperatures. Even very fast quenching (about 500 °C.s^{-1}) is not enough to limit B diffusion, and thus B segregation evolves during quenching. Therefore, the equilibrium B distribution reached at high soaking temperature cannot always be observed at room temperature.
(3) The ratio between boron segregated at γGBs and boron in solution in grains decreases with increasing temperature, following the classical equilibrium segregation equation. The concept of non-equilibrium segregation is not needed to explain our experimental observations.
(4) The increase of boron excess at γGBs with increasing soaking temperature originates from the austenite bulk enrichment in solute boron due to the dissolution of boron-containing precipitates. Segregation follows the classical equilibrium isotherms.
(5) The boron segregation enthalpy at austenite grain boundaries is −0.39 eV.

Declaration of Competing Interest

The authors declare that they have no known competing financial interests or personal relationships that could have appeared to influence the work reported in this paper.

Acknowledgments

The authors would like to thank Pr. M. Gouné for fruitful discussions. This project was supported by the National Association of Research and Technology, France (ANRT Project n_ 485-2014).

References

[1] M. Ueno, K. Itoh, The optimum condition to obtain the maximum hardenability effect of boron, Tetsu-to-Hagané 74 (1988) 910–917.
[2] X.L. He, Y.Y. Chu, J.J. Jonas, Grain boundary segregation of boron during continuous cooling, Acta Metall. 37 (1) (1989) 147–161.
[3] X.L. He, M. Djahazi, J.J. Jonas, J. Jackman, The non-equilibrium segregation of boron during the recrystalization of Nb-treated HSLA steels, Acta Metall. Mater. 39 (10) (1991) 2295–2308.
[4] T. Hara, H. Asahi, R. Uemori, H. Tamehiro, Role of combined addition of niobium and boron and of molybdenum and boron on hardnenability in low carbon steels, ISIJ Int. 44 (8) (2004) 1431–1440.
[5] D.J. Mun, E.J. Shin, K.C. Cho, J.S. Lee, Y.M. Koo, Cooling rate dependence of boron distribution in low carbon steel, Metall. Mater. Trans. A 43 (5) (2012) 1639–1648.
[6] Y.J. Li, D. Ponge, P. Choi, D. Raabe, Atomic scale investigation of non-equilibrium segregation of boron in a quenched mo-free martensitic steel, in: Proceedings of the 1st International Conference on Atom Probe Tomography and Microscopy, 159, 2015, pp. 240–247.
[7] Y.J. Li, D. Ponge, P. Choi, D. Raabe, Segregation of boron at prior austenite grain boundaries in a quenched martensitic steel studied by atom probe tomography, Scr. Mater. 96 (2015) 13–16.
[8] K. Zhu, C. Oberbillig, C. Musik, D. Loison, T. Iung, Effect of B and B+Nb on the bainitic transformation in low carbon steels, Mater. Sci. Eng. A 528 (12) (2011) 4222–4231.
[9] J.E. Morral, T.B. Cameron, A model for ferrite nucleation applied to boron hardenability, Metall. Trans. A 8 (11) (1977) 1817–1819.
[10] S. Yoshida, K. Ushioda, J. Ågren, Kinetic model of the γ to α phase transformation at grain boundaries in boron-bearing low-alloy steel, ISIJ Int. 54 (3) (2014) 685–692.
[11] R.G. Faulkner, Combined grain boundary equilibrium and non-equilibrium segregation in ferritic/martensitic steels, Acta Metall. 35 (12) (1987) 2905–2914.
[12] X.L. He, Y.Y. CHU, J.J. Jonas, Grain boundary segregation of boron during continuous cooling, Acta Metall. 37 (1989) 147–161.
[13] D. McLean, Grain Boundaries in Metals, Oxford Univ. Press, London, 1957.
[14] K.T. Aust, R.E. Hanneman, P. Niessen, J.H. Westbrook, Solute induced hardening near grain boundaries in zone refined metals, Acta Metall. 16 (3) (1968) 291–302.
[15] T.R. Anthony, R.E. Hanneman, Non-equilibrium segregation of impurities in quenched dilute alloys, Scr. Metall. 2 (11) (1968) 611–614.
[16] X. Tingdong, C. Buyuan, Kinetics of non-equilibrium grain-boundary segregation, Prog. Mater. Sci. 49 (2) (Jan. 2004) 109–208.
[17] X. Tingdong, S. Shenhua, S. Huazhong, W. Gust, Y. Zhexi, A method of determining the diffusion coefficient of vacancy-solute atom complexes during the segregation to grain boundaries, Acta Metall. Mater. 39 (12) (Dec. 1991) 3119–3124.
[18] H. Asahi, Effects of mo addition and austenitizing temperature on hardenability of low alloy B-added steels, ISIJ Int. 42 (10) (2002) 1150–1155.
[19] B. Hwang, D.-W. Suh, S.-J. Kim, Austenitizing temperature and hardenability of low-carbon boron steels, Scr. Mater. 64 (12) (Jun. 2011) 1118–1120.
[20] G. Shigesato, T. Fujishiro, T. Hara, Grain boundary segregation behavior of boron in low-alloy steel, Metall. Mater. Trans. A 45 (4) (Apr. 2014) 1876–1882.
[21] X.L. He, Y.Y. Chu, J.J. Jonas, The grain boundary segregation of boron during isothermal holding, Acta Metall. 37 (11) (Nov. 1989) 2905–2916.
[22] N. Valle, J. Drillet, A. Pic, H.-N. Migeon, Nano-SIMS investigation of boron distribution in steels, Surf. Interface Anal. 43 (1–2) (Jan. 2011) 573–575.
[23] J. Drillet, N. Valle, T. Iung, Nanometric scale investigation of phase transformations in advanced steels for automotive application, Metall. Mater. Trans. A 43 (13) (Dec. 2012) 4947–4956.
[24] J.B. Seol, N.S. Lim, B.H. Lee, L. Renaud, C.G. Park, Atom probe tomography and nano secondary ion mass spectroscopy investigation of the segregation of boron at austenite grain boundaries in 0.5 wt% carbon steels, Met. Mater. Int. 17 (3) (Jun. 2011) 413–416.
[25] F. Christien, C. Downing, K.L. Moore, C.R.M. Grovenor, Quantification of grain boundary equilibrium segregation by nanosims analysis of bulk samples: how to quantify grain boundary segregation using nanosims, Surf. Interface Anal. 44 (3) (Mar. 2012) 377–387.
[26] J. Takahashi, K. Ishikawa, K. Kawakami, M. Fujioka, N. Kubota, Atomic-scale study on segregation behavior at austenite grain boundaries in boron- and molybdenum-added steels, Acta Mater. 133 (Jul. 2017) 41–54.
[27] S. Watanabe, H. Ohtani, T. Kunitake, The influence of hot rolling and heat treatments on the distribution of boron in steel, Tetsu-to-Hagané 62 (1976) 1842–1850.
[28] S. Watanabe, H. Ohtani, T. Kunitake, The influence of dissolution and precipitation behavior of M23 (C, B)6 on the hardenability of boron steels, Trans. Iron Steel Inst. Jpn. 23 (2) (1983) 120–127.
[29] H. Tamehiro, M. Murata, R. Habu, M. Nagumo, Optimum microalloying of niobium and boron in hsla steel for thermomechanical processing, Trans. Iron Steel Inst. Jpn. 27 (2) (1987) 120–129.
[30] F. Han, B. Hwang, D.-W. Suh, Z. Wang, D.L. Lee, S.-J. Kim, Effect of molybdenum and chromium on hardenability of low-carbon boron-added steels, Met. Mater. Int. 14 (6) (2008) 667–672.
[31] L. Sangely, et al., CHAPTER 15. secondary ion mass spectrometry, in: T. Prohaska, J. Irrgeher, A. Zitek, N. Jakubowski (Eds.), New Developments in Mass Spectrometry, Royal Society of Chemistry, Cambridge, 2014, pp. 439–499.
[32] H.W. Werner, Quantitative secondary ion mass spectrometry: a review, Surf. Interface Anal. 2 (2) (Apr. 1980) 56–74.
[33] B.W. Krakauer, D.N. Seidman, Absolute atomic-scale measurements of the Gibbsian interfacial excess of solute at internal interfaces, Phys. Rev. B 48 (9) (Sep. 1993) 6724–6727.
[34] P. Maugis, K. Hoummada, A methodology for the measurement of the interfacial excess of solute at a grain boundary, Scr. Mater. 120 (Jul. 2016) 90–93.
[35] P. Felfer, B. Scherrer, J. Demeulemeester, W. Vandervorst, J.M. Cairney, Mapping interfacial excess in atom probe data, in: Proceedings of the 1st International Conference on Atom Probe Tomography and Microscopy, 159, Dec. 2015, pp. 438–444.
[36] Z. Peng, et al., An automated computational approach for complete in-plane compositional interface analysis by atom probe tomography, Microsc. Microanal. (2019) 1–12.
[37] H. Ohtani, M. Hasabe, K. Ishida, Calculation of fe-c-b ternary phase diagram, Trans. Iron Steel Inst. Jpn. 28 (1988) 1043–1050.
[38] X.P. Shen, R. Priestner, Effect of boron on the microstructure and tensile properties of dual-phase steel, Metall. Trans. A 21 (9) (Sep. 1990) 2547–2553.
[39] C. Philippot, K. Hoummada, M. Dumont, J. Drillet, V. Hebert, P. Maugis, Influence of a 2-D defect on the partitioning during the formation of a cementite particle in steels, Comput. Mater. Sci. 106 (Aug. 2015) 64–68.
[40] T. Fujishiro, T. Hara, G. Shigesato, Effect of mo on γ to α transformation and precipitation behavior in B-added steel, Tetsu–Hagane 101 (5) (2015) 300–307.
[41] P.E. Busby, M.E. Warga, C. Wells, Diffusion and solubility of boron in iron and steel, JOM 5 (1953) 1463–1468.
[42] T. Heumann, H. Mehrer, Diffusion in Metallen, Springer-Verlag, 1992.
[43] A. Janotti, M. Krčmar, C.L. Fu, R.C. Reed, Solute diffusion in metals: larger atoms can move faster, Phys. Rev. Lett. 92 (2004).
[44] W. Wang, S. Zhang, X. He, Diffusion of boron in alloys, Acta Metall. Mater. 43 (4) (Apr. 1995) 1693–1699.
[45] C. Wells, W. Batz, R.F. Mehl, Diffusion coefficient of carbon in austenite, J. Met. 188 (1950) 553–560.
[46] J. Dudala, J. Gilewicz-Wolter, Z. Stegowski, Simultaneous measurement of Cr, Mn and Fe diffusion in chromium-manganese steels, Nukleonika 2 (2005) 67–71.
[47] H. Jürgen Grabke, E. Marie Petersen, Diffusivity of nitrogen in iron-nickel alloys, Scr. Metall. 12 (12) (Dec. 1978) 1111–1114.
[48] F.S. Buffington, K. Hirano, M. Cohen, Self diffusion in iron, Acta Metall. 9 (5) (May 1961) 434–439.
[49] T.M. Williams, A.M. Stoneham, D.R. Harries, The segregation of boron to grain boundaries in solution-treated type 316 austenitic stainless steel, Met. Sci. 10 (1) (Jan. 1976) 14–19.
[50] S. Brotzmann, H. Bracht, Intrinsic and extrinsic diffusion of phosphorus, arsenic, and antimony in germanium, J. Appl. Phys. 103 (3) (Feb. 2008) 033508.
[51] A. Portavoce, O. Abbes, Y. Rudzevich, L. Chow, V. Le Thanh, C. Girardeaux, Manganese diffusion in monocrystalline germanium, Scr. Mater. 67 (3) (Aug. 2012) 269–272.
[52] I. Langmuir, THE adsorption of gases on plane surfaces of GLASS, mica and platinum, J. Am. Chem. Soc. 40 (9) (Sep. 1918) 1361–1403.
[53] P. Lejcek, Grain Boundary Segregation in Metals, Springer Series 136 (2010).
[54] M. Gouné, F. Danoix, S. Allain, O. Bouaziz, Unambiguous carbon partitioning from martensite to austenite in Fe–C–Ni alloys during quenching and partitioning, Scr. Mater. 68 (12) (Jun. 2013) 1004–1007.
[55] G. Da Rosa, P. Maugis, J. Drillet, V. Hebert, K. Hoummada, Co-segregation of boron and carbon atoms at dislocations in steel, J. Alloys Compd. 724 (Nov. 2017) 1143–1148.
[56] Z.N. Abdellah, R. Chegroune, M. Keddam, B. Bouarour, L. Haddour, A. Elias, The phase stability in the fe-b binary system: comparison between the interstitial and substitutional models, Defect Diffus. Forum 322 (Mar. 2012) 1–9.
[57] J.E. Morral, J. Jandeska, The binding energy of boron to austenite grain boundaries as calculated from autoradiography, Metall. Trans. A 11A (1980) 1628.
[58] R.G. Faulkner, Non-equilibrium grain-boundary segregation in austenitic alloys, J. Mater. Sci. 16 (1981) 373–383.
[59] G. Miyamoto, A. Goto, N. Takayama, T. Furuhara, Three-dimensional atom probe analysis of boron segregation at austenite grain boundary in a low carbon steel - Effects of boundary misorientation and quenching temperature, Scr. Mater. 154 (Sep. 2018) 168–171.